LA-UR-08- 00423

Approved for public release;
distribution is unlimited.

Title:	Statistics of Particle Concentration in Free-Surface Turbulence
Author(s):	M.M. Bandi, J. Larkin, W. Goldburg
Intended for:	Phys. Rev. E

Los Alamos
NATIONAL LABORATORY
EST. 1943

Form 836 (7/06)

Statistics of particle concentration in free-surface turbulence.

M. M. Bandi,[1,*] Jason Larkin,[2] and Walter I. Goldburg[3]

[1] *Center for Nonlinear Studies and Condensed Matter & Thermal Physics Group, Los Alamos National Laboratory, Los Alamos, NM 87545, USA.*

[2] *Department of Mechanical Engineering & Material Science, University of Pittsburgh, Pittsburgh, PA 15260, USA.*

[3] *Department of Physics & Astronomy, University of Pittsburgh, Pittsburgh, PA 15260, USA.*

(Dated: January 19, 2009)

Particles on the surface of an incompressible fluid maintained in a turbulent steady-state cluster into spatio-temporally complex flow structures. We experimentally study the statistics of particle concentration $n(r,t)$ over various coarse-grained scales r in the inertial range. Another control parameter is the Taylor Microscale Reynolds number Re_λ. The focus is on the steady state probability density function $\Pi(n_r)$. Attention is also given to the variance $\sigma^2(r,t)$ of this PDF, since it yields information about the topology of the coagulated structures. Where possible, the results are compared and contrasted with those obtained in a recent analytical and numerical study of two-dimensional synthetic turbulence by Ducasse and Pumir [1]. There, but not here, the dimensionless compressibility C is an important control parameter.

PACS numbers: 47.27.-i, 47.27.ed, 47.52.+j

I. INTRODUCTION

Understanding tracer advection in a turbulent flow is of practical interest in areas as diverse as pollutant transport, cloud formation due to inertial clustering, and dispersion of flotsam and phytoplankta at the ocean surface [2, 3]. Whereas turbulent mixing and dispersion of passive tracers in incompressible flows has been studied for long [4, 5], the preferential clustering of particles due to inertial effects or boundary conditions that lead to an effective compressibility has invited theoretical and experimental scrutiny only in recent times [1, 6–12].

Here we consider the Lagrangian evolution of tracer concentrations at the two-dimensional air-water interface. Although the underlying turbulence is incompressible, the particles which are lighter than water, are constrained to move only along the two-dimensional surface; they cannot follow water into the bulk. The tracers flee fluid upwellings (sources) and cluster into string-like structures along fluid downwellings (sinks) and form a compressible system. Inertial particles, such as raindrops in a storm, cluster because they are too massive to follow the local flow in which they move. In the present case of free-surface turbulence, even inertia-free particles will cluster because their motion is confined to the air-water interface. Despite this essential difference, properties of clusters in free-surface flows share many similarities with their inertial counterparts [9, 13]. This similarity is perhaps not surprising if one interprets the constrained motion of particles along the two-dimensional surface as an effective inertia that acts only along the third dimension (vertically into the bulk).

A quantitative measure of clustering in isotropic free-surface flows is the effective compressibility of the floaters, C:

$$C = \frac{\langle (\nabla \cdot \mathbf{v})^2 \rangle}{\langle (\partial_x v_x)^2 + (\partial_x v_y)^2 + (\partial_y v_x)^2 + (\partial_y v_y)^2) \rangle} \qquad (1)$$

For isotropic turbulence this parameter lies between 0 (incompressible fluids) and unity (potential flows). Past experiments and Direct Numerical Simulations (DNS) have consistently measured $C = 1/2$ at the free-surface [6].

Though the floaters move on an almost flat surface, their motion is not the same as incompressible turbulent flows in two dimensions. In 2D incompressible flows both the mean kinetic energy $\langle E \rangle$ and mean square vorticity or enstrophy $\langle \Omega^2 \rangle$ is conserved in the inertial range where (by definition of this range), the effect of viscosity can be ignored. The floaters, on the other hand, merely sample the incompressible 3D turbulence at the air-water interface, taken as the plane $(x, y, z = 0)$. At all spatial scales the floaters are driven apart by upwellings of the underlying fluid and coagulate at points where this flow is downward. Of course, these points of upwellings and downwellings fluctuate in space and time. The net effect on the floaters is the formation of string-like structures [6].

In face of these theoretical difficulties, further progress has been made by treating the floaters as a dynamical system coupled to an incompressible turbulent reservoir [7–12]. Theoretical advances have concentrated on the similarities shared by the free-surface particles with inertial particle dynamics. These theories [8, 10] specifically exploit the statistical properties of stretching fields of fluids that exist at the smallest spatial scales (below the Kolmogorov scale η, Table I). In the inertial range of turbulence where the velocity field is rough, theoreti-

the best approach seems to be to provide direct empirical evidence from experiments and simulations by tuning appropriate control parameters in aid of theory. In this vein Ducasse et. al. studied the statistics of preferential concentration in numerical simulations of synthetic free-surface turbulence with the effective compressibility C as their tuning parameter [1].

Here we study the concentration statistics of particle clusters in free-surface flows as a function of the Taylor Microscale Reynolds number (Re_λ). The compressibility C is not a free control parameter in the experiments discussed here. Rather, experiments and simulations show it to be $C \simeq 0.5$ [6, 7], thus making particles at the free-surface a strongly compressible system. Our interest lies in studying the general statistical features of particle clusters for both transient and steady-state evolution.

The topological structure of the clustering floaters is studied by measuring their two-dimensional density n_r averaged over a dimensionless length scale $r = s/\eta$, where s is the coarse-grained length scale and η is the measured dissipative scale of the turbulence (Table I). A visualization of the concentration $n_r(t)$ can be seen in Fig. 1. It is clear to the eye that the particles cluster along line-like structures. Because the underlying turbulence drives their motion, the positions of the floaters fluctuate in time and space. Hence the n_r is a random variable whose probability density function (PDF) $\Pi(n_r)$ can be measured. The variance $\sigma^2(r) = \langle (n_r - \langle n_r \rangle)^2 \rangle$ of this PDF is particularly amenable to interpretation. As for the first moment $\langle n_r \rangle$, it is normalized so that $\langle n_r \rangle$=1, making $\sigma^2(r) = \langle n_r^2 \rangle$-1. For scale-free particle distributions,

$$\sigma^2(r) \propto r^{-\alpha}. \qquad (2)$$

If the distribution of the floaters is uniform, $\alpha = 0$. In the opposite limit, where the particles cluster into points, $\alpha = 2$, since the embedding dimension here is 2. If the particles cluster into lines, $\alpha = 1$. In this experiment, α turns out to fall between 0 and 1.

The Experiment section explains the setup and Lagrangian interpolation scheme employed in the analysis followed by the Results section where we discuss the transient evolution of the statistics of preferential particle concentration and the concentration statistics in the stationary-state. Finally we summarize the results in the Summary section.

EXPERIMENT

The experiments were carried out in a tank 1m × 1m in lateral dimensions. It was filled with water to a depth of 30 cm. Turbulence is generated by a pump (8 hp)

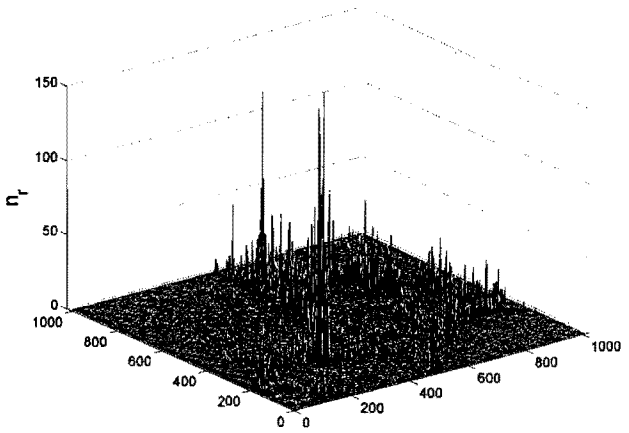

FIG. 1: Visualization of particle concentration $n_r(t = 1.5s)$ showing a strong non-uniformity at Re_λ=169. The spatial units are in pixels with 1 pixel $\simeq 0.01cm$. The coagulation occurs within several large-eddy-turnover-times τ_0 (Table I.)

that draws water from the tank and re-circulates it back through a system of 36 rotating jets placed horizontally across the tank floor. This system ensures that the source of turbulent injection is far removed from the free-surface where the measurements are made. More importantly, it minimizes the amplitude of surface waves which are unavoidable. The maximum amplitude of waves generated at the surface does not exceed 0.5 mm [6]. Further evidence that wave motion is not responsible for the effects reported here, come from simulations where wave motion is totally absent [6]. Those simulations are in very good agreement with prior laboratory experiments, where many aspects of floater coagulation were studied [6].

There are several issues to be mindful of in this experiment. First is the role of surface impurities in the form of an amphiphile layer that can cover the air-water interface. The experiment cannot be performed in the presence of these surface impurities. They suppress the coagulation seen in Fig. 1. Therefore, just prior to each experimental run, the surface is cleaned by skimming off the impurities. The second concerns the meniscus between the particles and the air-water interface and the role they play via capillary interactions as studied in [10, 14]. The particles chosen are hydrophilic and any such effects arising from capillary interactions between particles are very small compared to the turbulent intensity of the flow. Finally, as a test of the non-inertial character of the particles, we calculate their Stokes number St. In order to be considered non-inertial, St for the particles must be much less than unity [15]. In the experiments discussed here, $St \simeq 0.1$.

The turbulent parameters that characterize the various

in Table I. During a typical run, particles are constantly seeded into the fluid from the tank floor. They undergo turbulent mixing as they rise due to buoyancy and are uniformly dispersed by the time they rise to the surface. Once at the free-surface, their motion is constrained to the two-dimensional plane; they cannot return to the bulk. Therefore they cluster at the fluid sinks. This scheme of particle injection ensures that both sources and sinks of fluid receive equal coverage of particles on the surface. Furthermore, the constant seeding is necessary to replace any particles that leave the field of view during the experiment. A laser beam from a solid-state laser (5.5 W) is passed through a cylindrical lens to generate a sheet that grazes the surface. The 50 μm floaters then scatter the incident laser light. The positions and velocities of the particles are captured by a high-speed camera (Phantom v.5), which is suspended vertically above the tank. Typically the frame speed was set at 100 Hz.

The camera field-of-view is a square area of side length L $\simeq$ 9 cm. Its height above the water surface was chosen so that a pixel size is roughly 0.1 mm. This length is comparable to the dissipative scale of the turbulence (See Table I). The camera images are stored in a computer and subsequently fed into a particle tracking program developed inhouse. This particle imaging velocimetry (PIV) program takes a consecutive pair of images and correlates individual particles to generate an instantaneous velocity field of the turbulent free-surface. The temporal record of velocity fields is then fed into a Lagrangian tracking program that solves the advection equation for a set of computer generated (massless) particles $i = 1...m$ that are tracked in the Lagrangian frame of reference:

$$\frac{d\mathbf{x}_i}{dt} = \mathbf{v}(\mathbf{x}_i(t), t), \tag{3}$$

where $\mathbf{v}(\mathbf{x}_i, t)$ is the velocity field and $\mathbf{x_i} = (x_i, y_i)$. The camera software enables one to construct the tracks $\mathbf{x}_i(t)$ of the i^{th} floater in the camera's field of view. By trial and error the minimum number of Lagrangian particles required to obtain good statistics is 30,000/frame. We evolved 3×10^5/frame Lagrangian particles for each experimental run in order to ensure high statistical significance for the data. For each data set, a uniform distribution of Lagrangian tracers is generated at time t = 0 s (where $\alpha = 0$ in Eq. (2)) and evolved using Eq. 3. The concentration statistics are collected at each time-step by coarse-grained the domain at the chosen spatial scale $r = s/\eta$. Unlike the study of synthetic turbulence in [1], the compressibility is not adjustable.

RESULTS

It is first necessary to ensure that the spatial distribution of the floaters reaches a steady state. To do this,

TABLE I: Turbulent parameters measured at the experiment's surface.

Parameter	Expression	Measured Value
Taylor microscale λ (cm)	$\lambda = \sqrt{\frac{v_{rms}^2}{\langle(\partial v_x/\partial x)^2\rangle}}$	0.23-0.47
Taylor Re_λ	$\mathrm{Re}_\lambda = \frac{v_{rms}\lambda}{\nu}$	56-169
Integral Scale l_0 (cm)	$l_0 = \int dr \frac{\langle v_\parallel(x+r) v_\parallel(x)\rangle}{\langle (v_\parallel(x))^2\rangle}$	2.19-1.42
Large Eddy Turnover time τ_0 (s)	$\tau_0 = \frac{l_0}{v_{rms}}$	1.2-0.43
Dissipation Rate ϵ_{diss} (cm^2/s^3)	$\epsilon_{diss} = 10\nu \left\langle \left(\frac{\partial v_x}{\partial x}\right)^2 \right\rangle$	4.56-6.05
Kolmogorov scale η (cm)	$\eta = \left(\frac{\nu^3}{\epsilon}\right)^{1/4}$	0.022-0.020
RMS Velocity vrms (cm/s)	$v_{rms} = \sqrt{\langle v^2\rangle - \langle v\rangle^2}$	1.88-3.3
Compressibility C	$C = \frac{\left\langle \left(\vec{\nabla}_2 \cdot \vec{v}\right)^2 \right\rangle}{\left\langle \left(\vec{\nabla}_2 \vec{v}\right)^2 \right\rangle}$.	0.49 $\pm$0.03

$\sigma^2(r,t)$ was measured as a function of time to estimate when it reached its saturation value. Figure 2 shows that the variance saturates in a time of the order of several large-eddy turnover times $\tau_0 = l_0/v_{rms}$, where l_0 is the integral scale and v_{rms} is the rms velocity of the turbulence [16]. Both terms in the quotient are functions of the Re_λ, as seen in Table I. The inset of this figure shows that the saturation of $\sigma^2(r,t)$ is independent of the coarse-grained scale $r = s/\eta$ for all Re_λ. It is seen from Fig. 2 that $\sigma^2(t) \propto t^a$ with $a \simeq 1$, as it is in a random walk (solid straight line). The measurements presented subsequently are made in the steady-state, i.e. after the variance has saturated. Hence, the parameter t will be dropped.

Topological information about the floaters is gained by measuring $\sigma^2(r)$ as a function of the coarse-grained scale $r = s/\eta$. As noted above, if the variance obeys power-law behavior (eq. (2)), then the exponent α gives a quantitative measure of the topological structure. Figure 3 is a plot of the variance as a function of the coarse-grained scale r for the designated Re_λ. From this graph, it is apparent that α is less than unity and greater than 0, implying that the particle concentration has a complex structure between uniform ($\alpha = 0$) and line-like ($\alpha = 1$). The measurements are well-fitted with $\alpha \simeq 0.77$ for $Re_\lambda = 169$ for $0.8 \lesssim r \lesssim 8$. Because of experimental limitations, measurements were not made at $r \gtrsim 0.8$.

Having ascertained the time-scale to arrive at the steady-state, we now discuss the probability density func-

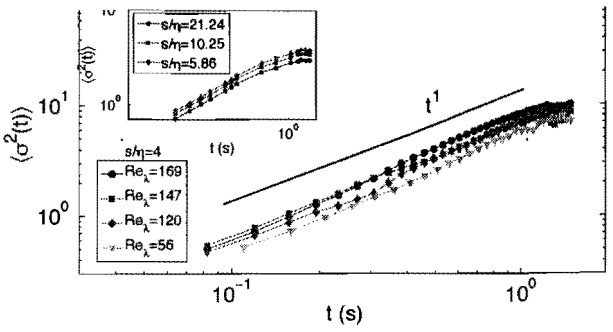

FIG. 2: Time evolution of the variance $\sigma^2(r,t)$ for $Re_\lambda = 56-169$. The inset shows $\sigma^2(r,t)$ for different coarse-grained scales $r = s/\eta$ for $Re_\lambda = 169$. These measurements show that $\sigma^2(r,t)$ is independent of Re_λ and r for $t \gtrsim 1s$ (Table I).

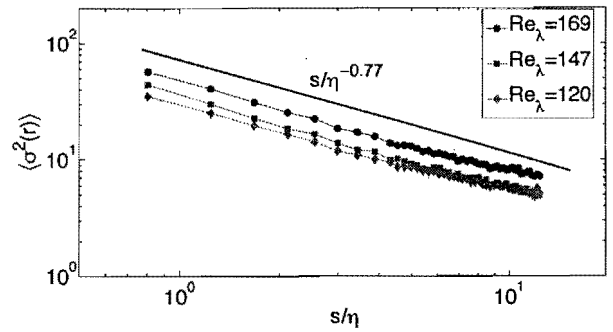

FIG. 3: Steady-state variance $\sigma^2(r)$ as a function of the dimensionless coarse-grained scale $r = s/\eta$ and Re_λ. The variance follows a power-law $n_r \propto r^{-\alpha}$ with $\alpha \simeq 0.77$ at the large Re_λ limit.

tion (PDF) $\Pi(n_r)$ of concentration. Probability density functions (PDF's) $\Pi(x)$ with power-law behavior are frequently encountered in nature. Examples include earthquakes, wars, and and solar flares [17]. They characterize the distribution of events x that are infrequent but of very large amplitude. This power-law $\Pi(x) \propto x^{-\gamma}$ is only observed over some limited range of x.

The immediate concern with power-law distributions is the convergence of the moments. Depending on the value of γ, the moments may diverge in the limits of small and large x. For finite systems, x is usually limited by some conservation law, causing the far wings of $\Pi(x)$ to decay faster than algebraically beyond some value of $|x| = \tilde{x}$. To determine $\tilde{x}$, it is often helpful to plot the cumulative distribution $\Pi_c(x)$ defined as

$$\Pi_c(x) = \int_x^\infty \Pi(x')dx'. \qquad (4)$$

If $\Pi(x) \propto x^{-\gamma}$, then $\Pi_c(x) \propto x^{1-\gamma}$.

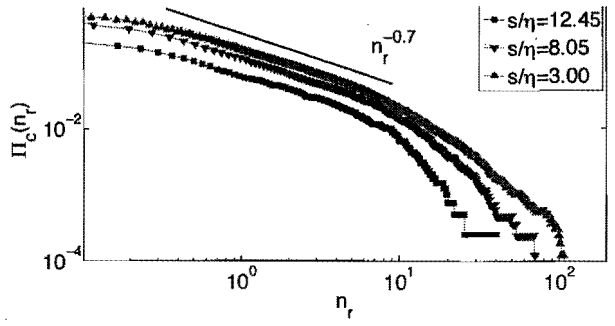

FIG. 4: Steady-state cumulative distribution $\Pi_c(n_r)$ for $Re_\lambda = 169$. At this maximum measured Reynolds number, the distribution follows a power-law $\Pi_c(n_r) \propto n_r^{1-\gamma}$, which is approximately independent of r. This algebraic behavior is only observed for $0.4 \lesssim n_r \lesssim 5$.

Figure 4 shows $\Pi_c(n_r)$ for $Re_\lambda = 169$ at various coarse-grained scales r. It is clear that $\Pi_c(n_r)$ can be fitted to a power-law $\Pi_c(n_r) \propto n_r^{1-\gamma}$ with $1-\gamma \simeq 0.7$ (solid line in the figure) for concentrations $0.4 \lesssim n_r \lesssim 5$. The exponent γ is also approximately independent of the coarse-grained scale r.

The value of $\gamma \simeq 1.7$ ensures that as $n_r \to 0$ the mean and variance of the distribution are bounded. In the limit of $n_r \to \infty$ the distribution has a cut-off which is faster than algebraic. It is apparent from the figure that this cut-off deceases with r. The independence of γ on the coarse-grained scale r is a departure from the results of Ducasse et al. [1], where the concentration PDF's depended on both r and the dimensionless compressibility.

Finally, Fig. 5 shows $\Pi_c(n_r)$ for the various Re_λ at a fixed scale $r = 5.2$. For Re_λ =56-120, the exponent γ characterizing the PDF is greater than 2. This implies that the mean will diverge in the lower limit. Of course these experimental data all have finite moments, but the scaling implies that more refined measurements will yield increasing values for the mean. For Re_λ =147-169 the exponent γ is less than 2, ensuring that the mean is bounded in the lower limit. Again, all distributions are bounded in the upper limit by a cut-off which is faster than algebraic. It appears that in the asymptotic limit of large Re_λ, the power-law behavior characterizing the distribution at the low concentrations has an exponent ensuring that the mean is bounded.

The synthetic turbulence analysis of DP yields very different results. There it is the low-density wing of $\Pi(n_r)$ that decays algebraically, while the positive wing has the more Gaussian shape. In this experiment, γ is independent of r, contrary to the results of DP [1]. The origin of this difference in $\Pi(n_r, r)$ likely has to do with the different role played by C in synthetic versus laboratory turbulence. In that study, particles evolved into point-like structures, while here, particles evolve to form line-

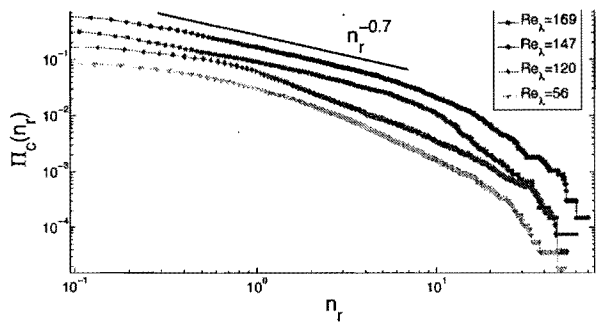

FIG. 5: Steady-state cumulative distributions for $Re_\lambda = 56 - 169$. In the large Re_λ limit the distributions follow power-laws which insure that the mean and variance are bounded in the lower concentration limit.

like structures. This numerical analysis of [1] is for small compressibilities $C \lesssim 0.05$. Because the compressibility is much larger in this experiment and in other experiments and simulations [6, 7], these results and the results of DP cannot be usefully compared.

V. SUMMARY

This experiment examines the spatial structure of particles that float on a turbulent sea. The particle density of the floaters, n_r is averaged over a range of scales r lying in the inertial range. The focus is on the two-dimensional probability density function $\Pi(n_r)$ and its variance $\sigma^2(r)$ after the steady state has been reached. In the initial state, at t =0, the particles are uniformly distributed, so that $\sigma^2(r)$ is independent of r. The measurements show, as does the eye, that the floaters cluster into a mixture of string-like structures where the variance $\sigma^2(r) \propto r^{-\alpha}$ with α lying between zero (uniform particle distribution) and unity (string-like structures). The exponent characterizing the power-law of the PDF is independent of r for the largest Re_λ reached in this experiment. With the distribution's exponent independent of r and the variance $\sigma^2(r)$ showing power-law behavior itself in the inertial range, only the distribution cut-off varies with r. This and Pumir [1], who used the coarse-grained scale r and compressibility C to collapse their distributions onto a single curve.

ACKNOWLEDGEMENTS

Funding was provided by the US National Science Foundation grant # DMR-0604477. This work was partially carried out under the auspices of the National Nuclear Security Administration of the U.S. Department of Energy at Los Alamos National Laboratory under Contract No. DE-AC52-06NA25396.

---

* Corresponding Author: mbandi@lanl.gov

[1] L. Ducasse and A. Pumir, Phys. Rev. E. **77**, 066304 (2008).
[2] R. A. Shaw, Annu. Rev. Fluid. Mech. **35**, 183 (2003).
[3] G. Falkovich, A. Fouxon, and M. G. Stepanov, Nature **419**, 151 (2002).
[4] L. F. Richardson, Proc. Roy. Soc. A **110**, 709 (1926).
[5] H. Stommel, J. Marine Res. **8**, 199 (1949).
[6] J. R. Cressman, J. Davoudi, W. I. Goldburg, and J. Schumacher, New J. Phys. **6**, 53 (2004).
[7] G. Boffetta, J. Davoudi, B. Eckhardt, and J. Schumacher, Phys. Rev. Lett. **93**, 134501 (2004).
[8] J. Bec, K. Gawedzki, and P. Horvai, Phys. Rev. Lett. **92**, 224501 (2004).
[9] G. Boffetta, J. Davoudi, and F. DeLillo, Europhys. Lett. **74**, 62 (2006).
[10] P. Denissenko, G. Falkovich, and S. Lukaschuk, Phys. Rev. Lett. **97**, 244501 (2006).
[11] M. M. Bandi, W. I. Goldburg, and J. R. Cressman, Europhys. Lett. **76**, 595 (2006).
[12] M. M. Bandi, J. R. Cressman, and W. I. Goldburg, J. Stat. Phys. **130**, 27 (2008).
[13] G. Falkovich and A. Pumir, Phys. Fluids **16**, L47 (2004).
[14] G. Falkovich, A. Weinberg, P. Denissenko, and S. Lukaschuk, Nature **435**, 1045 (2005).
[15] G. Boffetta, F. DeLillo, and G. Gamba, Phys. Fluids **16**, L20 (2004).
[16] U. Frisch, Cambridge University Press (1996).
[17] M. E. J. Newman, Contemporary Phys. **46**, 323 (2005).